Sensors and Materials, Vol. 11, No. 2 (1999) 111–130
MYU Tokyo

S & M 0360

Thin Film Shear Modulus Determination with Quartz Crystal Resonators

Ralf Lucklum, Carsten Behling and Peter Hauptmann

Otto-von-Guericke-University Magdeburg, Institute for Measurement Technology and Electronics (IPE), POB 4120, D-39016 Magdeburg, Germany

(Received April 18, 1998; accepted January 19, 1999)

Key words: acoustic sensors, materials science, quartz crystal resonators, shear modulus, thin films

The dependence of the electrical response of acoustic wave sensors on the viscoelastic properties of a coating material is used for the determination of the complex shear modulus of thin polymer films. In this paper we briefly discuss the underlying methodological background and analyze a composite quartz crystal resonator. We present results of experiments using a 1 μm Polyisobutylene (PIB) film at the fundamental quartz crystal frequency and the third and fifth harmonics. Both the glassy and the rubbery polymer consistency were investigated.

1. Introduction

Quartz crystals are widely used as frequency normals in modern electronics and as sensor elements, *e.g.* for the quartz crystal microbalance (QCM). These applications take advantage of the crystal's very high quality factor (Q-factor) and the high sensitivity of the mechanical eigenfrequency to surface mass changes. In chemical sensor applications, analyte sorption in a sensitive layer, which covers one or both surfaces of the quartz disc, results in a measurable surface mass change. In almost all of these applications, the quartz resonator works as the frequency-determining element of an electrical oscillator and the oscillating frequency is measured. The Q-factor of the sensor is still high, hence the oscillating frequency is very stable and can be measured with high resolution. The frequency change can be related to mass or thickness changes of the coating, or the analyte concentration in a gas. In QCM studies, it is assumed that the film is thin and rigidly

coupled to the underlying substrate, thereby allowing the interpretation of resonant frequency changes, Δf, as film mass or thickness.[1]

$$\Delta f = -\frac{2f_0^2}{NAZ_{cq}} m_f = -\frac{2f_0^2}{N \cdot Z_{cq}} \rho_f h_f \text{ or } \Delta f = -f_0 \frac{\rho_f h_f}{\rho_q h_q} \qquad (1a),(1b)$$

Z_{cq} is the characteristic quartz impedance (8.84 MPa s m^{-1}), N is the overtone number, m_f is the film mass, A is the electrode area, ρ is the density, and h is the thickness. Indices q and f indicate the quartz crystal and the film, respectively. The initial resonant frequency is commonly used for f_0. Equations (1a) and (1b) are the same if the mechanical resonant frequency is used for f_0.

The exposure of the resonator to a liquid medium results in an acoustic energy loss and hence in a decrease of the crystal's Q-factor. However, if the crystal vibrates in the thickness shear mode, the energy loss is not so severe as to preclude oscillation. A shear wave is launched into the liquid with decay length $\delta = \sqrt{\frac{\eta_l}{\pi f_0 \rho_l}}$ where ρ_l and η_l are the liquid density and liquid viscosity, respectively.[2] The frequency shift from contact with a semi-infinite Newtonian liquid is given by[3]

$$\Delta f = -\frac{2f_0^2}{Z_{cq}} \sqrt{\frac{\rho_l \eta_l}{4\pi f_0}}. \qquad (2)$$

The frequency shift resulting from a thin rigid layer and from the liquid contact is additive.[4] These investigations opened the way for the development of deposition monitors, gas sensors, *in situ* liquid studies, *e.g.*, the electrochemical quartz crystal microbalance (EQCM), QCM sensors for chemical liquid analysis and density-viscosity measurements. A modern application of surface-modified quartz resonators is the separate determination of liquid density and viscosity with a two-element concept.[5]

Recently, quartz resonators have become popular for the determination of material parameters of thin films that cover the quartz crystal surface.[6–9] This development is of special interest for the characterization of viscoelastic materials such as polymers. These materials respond to external forces in a manner intermediate between the behavior of an elastic solid and a viscous liquid. The modulus of viscoelastic materials is not a constant and depends strongly on the measuring temperature and the frequency of the applied dynamic force. Dynamic mechanical studies of thin viscoelastic films are difficult. The traditional equipment does not allow the investigation of films with μm thickness and does not allow high-frequency measurements in the MHz range. The investigation of the mechanical film properties is of basic interest in materials science, stimulated, *e.g.*, by the development of new materials, by the tendency towards miniaturization in the semiconductor industry, and by new technologies in surface modification.

Mechanical film properties can also influence the transduction mechanism of acoustic sensors in their 'classical' application as chemical QCM sensors. Viscoelastic effects can contribute significantly to the shift of the resonant frequency. This contribution depends on the shear modulus of the coating and the experimental setup[10–13] and should be known for the correct calculation of the deposited film thickness and mass of the absorbed analyte.

All the different applications of an acoustic sensor are based on the same physical background, the propagation of acoustic waves in a multilayer structure. The changes in the intrinsic material properties do not appear directly as linear changes in the electrical properties. They result from changes in the effective surface acoustic impedance seen from the resonator at its interface to the coating. We will show that the shear parameter determination with acoustic devices is applicable with sufficient accuracy under certain acoustic conditions. The experimental setup must be carefully adjusted to cover the part of interest of a broad range of possible polymer shear parameters. Coating thickness and measuring frequency play the dominant roles in such a process.

2. Viscoelastic Materials

The mechanical strength of a body is described by its modulus. In the case of a shear stress the shear modulus, G, is applied. A thick shear mode resonator generates a sinusoidal stress, σ, with the angular frequency, ω, in the attached body. If the material is of a viscoelastic nature, the strain, γ, will lag behind the stress by some amount. Quite often it is convenient to separate the viscoelastic response into in-phase and out-of-phase components. The in-phase and out-of-phase shear moduli, G' and G'', and the loss tangent, tan δ, are given as

$$G'' = \frac{\sigma'}{\gamma}, \; G'' = \frac{\sigma''}{\gamma} \text{ and } \tan\delta = \frac{G''}{G'}. \tag{3}$$

In-plane stress results in elastically stored energy which is completely recoverable, whereas one-fourth-cycle separated stress and strain results in the dissipation of energy, which is lost to the system. This behavior can be represented by complex numbers, giving rise to a complex shear modulus, $\underline{G}$:

$$\underline{G} = G' + \mathrm{j}\, G'', \tag{4}$$

where $\mathrm{j} = \sqrt{-1}$ is the imaginary unity. The behavior of viscoelastic materials subjected to oscillatory perturbations may also be treated by generalizing the concept of viscosity rather than the modulus. Newton's law becomes $\underline{\sigma} = \underline{\eta}\frac{\mathrm{d}\underline{\gamma}}{\mathrm{d}t}$, where $\underline{\eta} = \eta' + \mathrm{j}\eta''$. The relationship between these concepts is given by

$$\eta'(\omega) = \frac{G''(\omega)}{\omega} \text{ and } \eta''(\omega) = \frac{G'(\omega)}{\omega}. \quad (5)$$

The prominence of viscoelasticity in polymers is not unexpected due to their molecular structure. Four regions with very different material properties of linear amorphous polymers can be distinguished. In the glassy region the material is rigid. The shear storage modulus is about 10^9 Pa and decreases slowly with temperature. The shear loss modulus is significantly lower but increases with temperature. Molecular rearrangements on a long-range scale are severely restricted. Distortions generated by the external stress, being of a rather high energy, result in the high storage modulus.

The transition region can be found upon increasing the temperature. In a more or less broad temperature range (depending on the polymer) the modulus decreases several decades. G' and G'' are of the same order of magnitude, hence the loss tangent has a maximum. Reorientation of chain segments to lower energy conformations is possible, resulting in the decrease of the storage modulus. The region is referred to as the glass transition region and the corresponding temperature, as glass transition temperature, T_g.

In the rubbery state, all configurational modes of motion within the entanglement coupling points can freely occur. G' is on the order of 10^6 Pa and $G'' < G'$.

At still higher temperatures more and more chains can escape from topological restraints; this is the flow region.[14,15]

If the shear parameter determination is performed with an acoustic wave device, the much higher probing frequency must be taken into account. For example, at T_g, the material still exhibits glasslike behavior for the acoustic wave. A further increase in temperature is necessary for the relaxation processes corresponding to the rapid shear modulus decrease to be fast enough to take place within a period of oscillation. The transition temperature determined by a dynamic experiment is called the dynamic glass transition, T_α, to distinguish it from the static glass transition, T_g. This shift on the temperature scale as a result of the increased measuring frequency is a general phenomenon and can be described as the time-temperature correspondence principle of polymer relaxation.[14]

$$G(T_0,t) = G(T,t/a_T) \quad (6)$$

T_0 may act as reference temperature, a_T is the shift factor. The function $\log a_T$ exhibits similar behavior for all amorphous polymers and can be expressed as[16]

$$\log a_T = \log \frac{\omega_0}{\omega} = \frac{-C_1(T - T_g)}{C_2 + T - T_g}. \quad (7)$$

The constants, C_1 and C_2, are originally thought to be universal constants ($C_1 = 17.4$, $C_2 = 51.6$), however, C_1 is approximately constant whereas C_2 varies quite widely (*e.g.*, PIB: $C_1 = 16.6$, $C_2 = 104$).[17]

3. Acoustics

To calculate the shear parameters of a thin layer from the electrical response of a vibrating quartz crystal, we must consider the sensor as a composite resonator. It consists of a piezoelectric layer with multiple nonpiezoelectric layers in which an acoustic wave propagates. The piezoelectric quartz substrate is used for generating and detecting the acoustic wave. Changes in magnitude and phase of the electrical impedance or admittance indicate physical property changes occurring in the contacting nonpiezoelectric layers, including changes in the shear modulus of the film.

We derived the relation between the electrical sensor response and intrinsic and geometrical parameters of the film in a one-dimensional model from the solution of the wave equation.[9] This is a commonly accepted approximation. The high aspect ratio between the diameter of a quartz disc and the thickness of the crystal and the film thickness makes this assumption reasonable. However, it has been shown experimentally[18,19] and in a numerical two-dimensional model[20] that the real quartz exhibits effects which are mainly related to its finite lateral dimensions. The vibrational pattern at the surface of the quartz plate is one example. It has a maximum in the center of a circular electrode and decays toward the edge of the quartz disc.[18] An important consequence is the deviation of some quartz parameters from geometric or literature values.[20,21] We replace the geometric electrode area, and consequently the capacitance, C_0, formed by the electrodes, with an effective value to take the vibrational amplitude distribution into account. We also use an effective quartz viscosity to include other energy dissipation mechanisms. We substitute the thickness of the quartz crystal with an effective value which includes the contributions of both electrodes. This is carried out for simplicity. Both electrodes may also be considered as separate layers. The effective values are determined in a preceding step from the impedance curve of uncoated quartz. We assume that the changes of the effective values after the coating procedure are negligible. We analyzed the value of the effective area by FEM and found a reduction of about 0.4% after casting a 1 μm polymer film onto the electrode.[20] We took this deviation into account although it has no significant influence on the computed shear modulus.

Finally, under many experimental conditions, the film thickness is not perfectly uniform and thus it is replaced by an effective value which is calculated from the frequency shift before and after the coating procedure at a sufficiently low temperature where the polymer film is expected to behave like a rigid material. This acoustically effective film thickness may differ from results of other independent methods.[22] Although we must assume glassy film conditions, we found this method to have the highest accuracy.

The transmission line technique is convenient for modeling one-dimensional, multilayer structures. The impedance concept in acoustic wave propagation problems uses a chain matrix technique. All layers of the composite resonator act as transmission lines with finite length, h_i, and a complex wave propagation constant, $\underline{\gamma}_i = \mathrm{j}\,\dfrac{\omega}{\sqrt{\underline{G}_i / \rho_i}}$. The layers are assumed to be isotropic and uniform with a characteristic intrinsic acoustic impedance (index a) $Z_{ci}^{a} = \sqrt{\rho_i \underline{G}_i}$. For the piezoelectric quartz layer the electrical port must be

included as a third port. We use the KLM equivalent circuit to relate the mechanical vibration amplitude to the driving voltage.[23] This model consists of two cascaded transmission lines and is composed of distributed and lumped elements. The piezoelectricity is modeled by a transformer with the turn ratio $1{:}N$ and by the element jX. The complete transmission line model with a single polymer film (index p) which is used for the description of our experimental arrangement is shown in Fig. 1. The bottom quartz surface at port GH is stress free, corresponding to a short-circuited acoustic port. The upper surface is coated with the material to be investigated.

The following expression for the electrical impedance (index e), $\underline{Z}^e$, can be obtained:

$$\underline{Z}^e = Z_{AB} = \frac{1}{j\omega C_0} + jX + \frac{1}{N^2} Z_{CD}$$

$$= \frac{1}{j\omega C_0}\left(1 - \frac{\underline{K}_q^2}{\underline{\alpha}_q} \frac{2\tan(\underline{\alpha}_q / 2) - j\underline{\zeta}}{1 - j\underline{\zeta}\cot(\underline{\alpha}_q)}\right), \tag{8}$$

with $\underline{\zeta} = \underline{Z}_L^a / \underline{Z}_{cq}$, $\underline{K}_q^2 = \dfrac{e_q^2}{\varepsilon_q \cdot (c_q + j\omega\eta_q)}$ and $\underline{\alpha} = \omega \dfrac{h_q}{\underline{v}_q}$, where e_q, ε_q, c_q, η_q and $\underline{v}_q$ are the quartz piezoelectric constant, permittivity, piezoelectric stiffened elastic constant, viscosity and wave velocity, respectively.

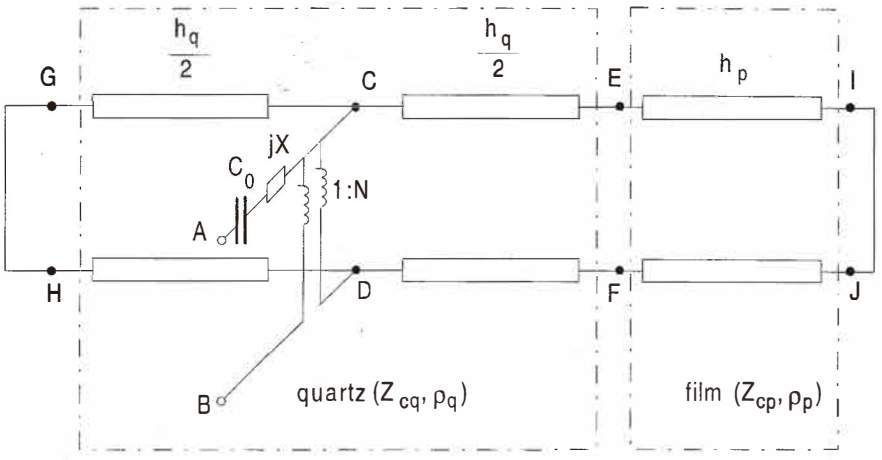

Fig. 1. Transmission-line model for a single piezoelectric layer (AT-quartz crystal, index q) and a single nonpiezoelectric layer (polymer, index p). The terminal surfaces of this composite resonator are assumed to be stress free, corresponding to a short-circuited acoustic port.

$\underline{Z}^e$ can be transformed into a parallel circuit consisting of a static capacitance, C_0, and the motional impedance, $\underline{Z}^e_m$, which itself can be split into two additive parts representing the uncoated quartz ($\underline{Z}_{m,q}$) and the transformed acoustic load ($\underline{Z}_{m,L}$):

$$\underline{Z}^e_m = \frac{1}{j\omega C_0}\left(\frac{\underline{\alpha}_q / \underline{K}_q^2}{2\tan(\underline{\alpha}_q / 2)} - 1\right) + \frac{1}{\omega C_0}\frac{\underline{\alpha}_q}{4\underline{K}_q^2}\frac{\underline{\zeta}}{1 - j\underline{\zeta}/(2\tan(\underline{\alpha}_q / 2))}. \tag{9}$$

Equation (9) is exact within the one-dimensional model. It can be applied without restrictions to the load on the quartz.[24] The motional load, $\underline{Z}_{m,L}$, and the acoustic load, $\underline{Z}^a_L$, are approximately proportional if $\underline{Z}^a_L << 2\underline{Z}_{cq}\tan(\underline{\alpha}_q / 2)$.

The acoustic load of a single viscoelastic polymer film (to indicate the polymer, we use the index p instead of the load index L) with finite thickness, h_p, and without an additional load at the surface, can be calculated as:

$$\underline{Z}^a_p = j(\rho_p \underline{G}_p)^{1/2}\tan\left(\omega\sqrt{\frac{\rho_p}{\underline{G}_p}}h_p\right) = j\underline{Z}_{cp}\tan\left(\omega\frac{\rho_p}{\underline{Z}_{cp}}h_p\right). \tag{10}$$

Equation (10) has general validity and is illustrated in Fig. 2. The complex acoustic impedance is separated into its imaginary (Figs. 2(a) and 2(c)) and real parts (Figs. 2(b) and 2(d)). The range of $\underline{G}$ values includes the glassy and rubbery states of polymers as discussed in the previous section. At the fundamental frequency (Figs. 2(a) and 2(b)) one can distinguish between a rather planar area at the right and the upper parts of the 3D diagrams and significant extremes in the lower left corner. The flat area is almost parallel to the zero plane, and the real part in that range is very small (less than 100 Pa s m^{-1}). This plane region reflects the validity range of the gravimetric regime of the quartz resonator. The length of the arrows hitting the flat area in Fig. 2(a) differ by less than 0.15%. They symbolize the frequency shift due to the presence of the 1 μm coating, which is proportional to $-\mathrm{Im}(\underline{Z}^a_p)$ in almost the whole range of G' and G''.[25] It includes the Sauerbrey requirement of a rigid film, which is fulfilled on the right side of the diagrams. Here, the material is in the glassy state. The additional lines represent $-\mathrm{Im}(\underline{Z}^a_p)$ at $G' = 10^9$ Pa for the third and the fifth harmonic. In agreement with eq. (1) the length of the arrows is 3 times (3rd harmonic) or 5 times (5th harmonic) the arrow length at the fundamental frequency.

The acoustic load generated due to the 1 μm polymer film in the rubbery state is totally different. $\mathrm{Im}(\underline{Z}^a_p)$ shows huge changes with changes in both G' and G''. The extremes are related to acoustic film resonance.[26] This is the viscoelastic regime of the quartz resonator. $\mathrm{Re}(\underline{Z}^a_p)$ is a measure of the attenuation of the quartz oscillation and increases

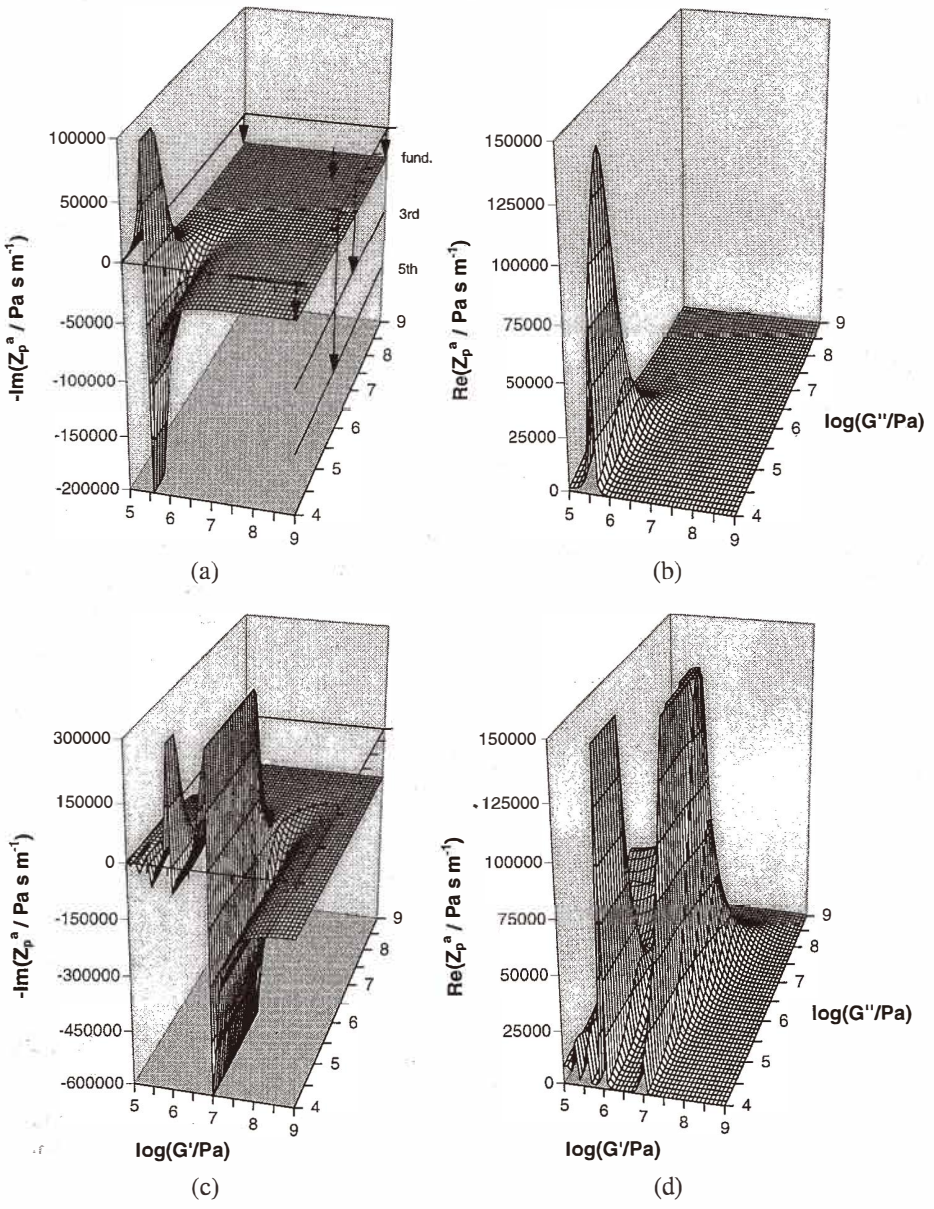

Fig. 2. Imaginary (a,c) and real (b,d) parts of the acoustic load of a single polymer layer of 1 μm thickness. The probing frequency is 5 MHz (a,b) and 25 MHz (c,d). The arrows in (a) indicate the shift of the planar area due to the presence of the polymer film on the blank quartz crystal surface at the fundamental frequency and the 5th harmonic. The arrow length is proportional to the frequency shift of the resonance frequency.

rapidly, just where $\mathrm{Im}(\underline{Z}_p^a)$ is very sensitive to changes in $\underline{G}$. However, this wave propagation phenomenon should not be confused with the acoustic energy loss.

It is obvious from Figs. 2(a), 2(b), and eq. (10) that film thickness and film shear modulus cannot be determined under the same experimental conditions. To determine the coating thickness, the acoustic load should be independent of $\underline{G}$. This is given for a small $\varphi = \omega\sqrt{\frac{\rho_p}{\underline{G}_p}}h_p$, i.e., small h_p and/or large $\underline{G}_p$, where the tan function can be approximated by its argument: $\underline{Z}_p^a = \mathrm{j}\omega\rho_p h_p$. To determine the film thickness of a rubbery film, the temperature should be decreased to achieve a glassy film consistency. To determine the shear modulus of a glassy material, either the film thickness or the probing frequency or both must be increased to obtain a sufficient large φ. The frequency dependence of the shear modulus should not be a problem as long as the probing frequency does not coincide with relaxation processes in the material. The effect of such a change in the experimental conditions on $\underline{Z}_p^a$ is shown in Figs. 2(c) and 2(d). In this example, the film thickness is left at 1 μm, and the oscillation frequency is increased to 25 MHz. The acoustic impedance behaves quite differently. At the fundamental frequency $\underline{Z}_p^a$ exhibits large planar areas in Figs. 2(a) and 2(b). By contrast, under the experimental conditions of Figs. 2(c) and 2(d) the remaining planar area is shifted downwards to the value indicated in Fig. 2(a) (note the different scaling of the ordinate), but at the same time, the extremes shift to higher values of G' and G'' and new extremes arise in the lower left region. The real part is small only in the glassy range and within small gaps between the maxima. The main maximum and the partly hidden 'crest' perpendicular to the main maximum is of special interest for the investigation of the glass transition because the paths of G' and G'' must cross this area.

Figure 3 shows a qualitative map of how sensitive $\underline{Z}_p^a$ responds to the shear storage and the shear loss modulus of a 1 μm polymer film at the fundamental frequency (5 MHz) and the 5th harmonic (25 MHz). It combines the opposite effect of a large gradient in $\mathrm{Im}(\underline{Z}_p^a)$ and a high $\mathrm{Re}(\underline{Z}_p^a)$, separated into G' and G''. The darker the grey color, the better the response. All four cases show quite different results. As predicted from Fig. 2 the shear modulus can be determined in a limited range which depends on the relation between coating thickness and probing frequency. The requirements for a successful shear modulus calculation are fulfilled in a significantly broader range for the storage modulus, G', at both the fundamental frequency (Fig. 3(a)) and the 5th harmonic (Fig. 3(c)). The acoustic load responds to the storage modulus even at glassy G values at the fundamental frequency. $\underline{Z}_p^a$ is sufficiently sensitive to G'' only if the film is in the rubbery state or in the transition range (Figs. 3(a) and 3(b)). If the film is probed with a 25 MHz acoustic wave, the glassy state is more accessible. At this stage, film resonances hinder the analysis of the rubbery state (Figs. 3(c) and 3(d)).

Based on these analyses, the electrical impedance is expected to be sufficiently sensitive to the complex film shear modulus at the fundamental frequency and $\underline{G}$ values

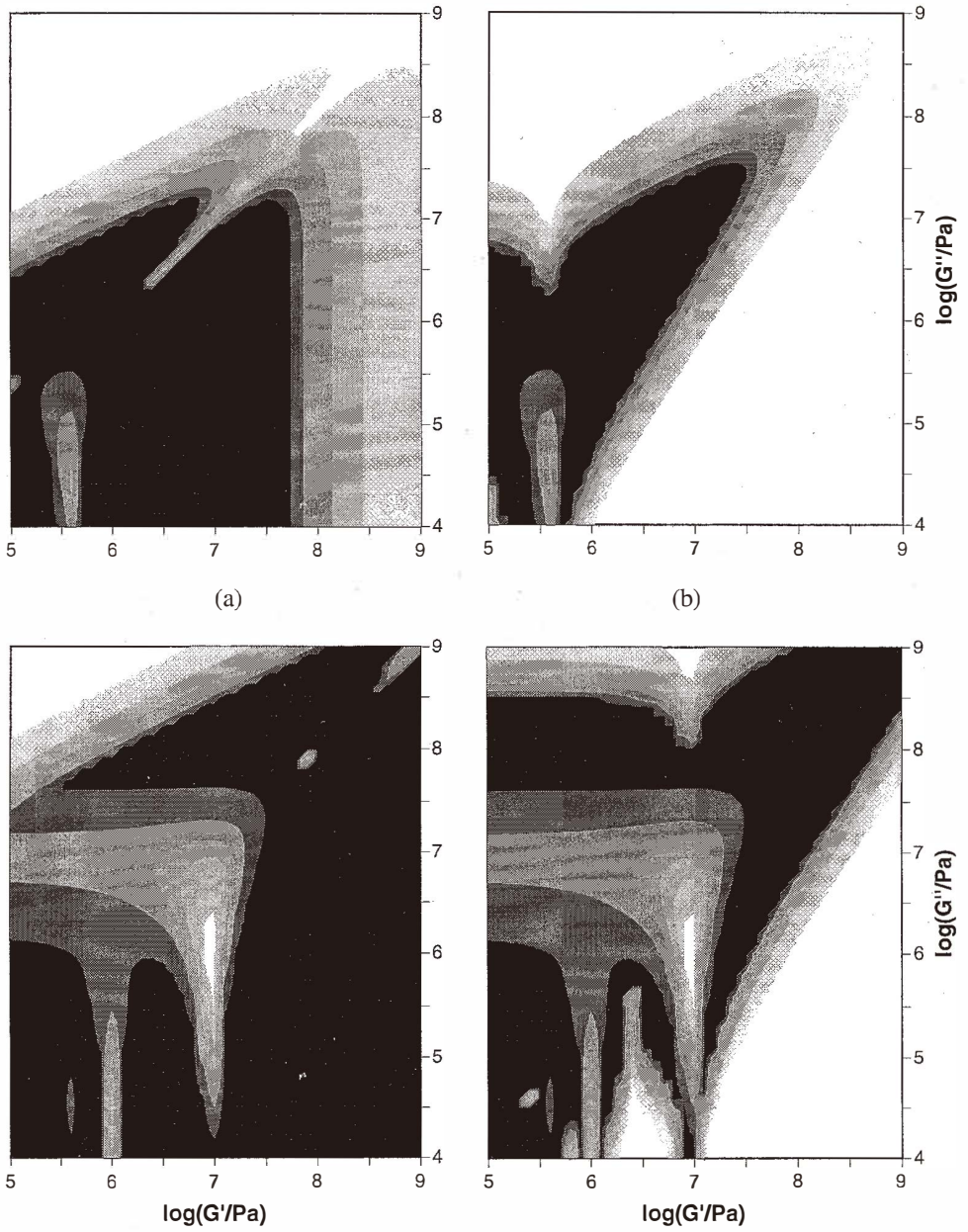

Fig. 3. Map of sensitivity of $\underline{Z}_\rho^a$ to changes in the shear storage modulus (a,c) and the shear loss modulus (b,d) at the fundamental frequency (a,b) and the 5th harmonic (c,d). The darkness of the gray increases with the sensitivity of the acoustic device.

typical of a material in the transition range and rubbery state. At higher harmonics, the quartz should respond significantly to shear modulus changes in the glassy state of the film. We, furthermore, expect a highly damped oscillation of a quartz with a 1 μm rubbery coating at the 5th harmonic. The shear storage modulus should be calculated in an extended material parameter range.

4. Experimental Details

Polyisobutylene (PIB), obtained from Aldrich, with a medium molecular weight of 380,000, a density of 0.92 g/cm^3, and a static glass transition temperature $T_g = -68$°C, has been examined.

All experiments were performed using a polished 5 MHz AT-cut quartz crystal (Maxtek, Torrance, CA) of 2.54 cm diameter. The electrode geometry contains a 12.9 mm-diameter grounded electrode on one side, while the other side contains a 6.6 mm-diameter electrode which is at the RF potential.

The quartz crystal was mounted in a measuring cell and electrically contacted with pin contacts. The parasitic contact resistance and capacitance have been taken into account during the calibration at room temperature and the fitting of measured impedance data. A constant flow of dry nitrogen was supplied to prevent any influence of humidity. The whole cell was mounted in a temperature test chamber (Tenney Environmental, Parsippany, NJ, USA). The temperature was controlled with a thermocouple in the measuring cell adjacent to the quartz crystal. The temperature was increased from -50°C to 150°C at 0.26 K min^{-1}. A HP 8752A (Hewlett-Packard) network analyzer was used to measure the complex reflection coefficient directly at the quartz contacts. This value is related to the electrical impedance by

$$\underline{S}_{11} = \frac{\underline{Z}_i^e - Z_0}{\underline{Z}_i^e + Z_0}, \tag{11}$$

where Z_0 is 50 Ω. Measurements were performed 3 times at 801 points centered about the fundamental, third- and fifth-harmonic resonant frequencies.

The polymers were prepared by spin-casting onto the resonator at 1,500 rpm from a solution in chloroform/toluene mixture. The solvent was driven off during a postannealing process at 150°C for at least 30 min. The resulting film thickness was about 1 μm. It was optimized with regard to the glass transition.

Every experiment started with a scan of the uncoated quartz crystal at every 5 K for the fundamental frequency, the 3rd and the 5th harmonic. It was followed by the coating procedure. The coated device was scanned with the same procedure as for the uncoated quartz. The measurement was automatically controlled and recorded using HP VEE for Windows (Hewlett-Packard).

5. Results and Discussion

5.1 *Film thickness determination*

The (effective) coating thickness necessary for unambiguous determination of the shear modulus must be measured under glassy polymer conditions. It was calculated from the resonant frequency at – 50°C after film deposition for every harmonic. Although this temperature is higher than the static glass transition temperature of PIB, it is sufficiently low at 5 MHz (see eq. (7)). The uncoated quartz was also measured at the cooled temperature to account for the temperature dependence of the resonator properties. We analyzed the theoretical thickness errors from different approximations.[25] The thickness error depends on the kind of oscillator used to excite the quartz or on which characteristic frequency (zero-phase frequencies, impedance minimum or impedance maximum frequencies) was selected from the impedance plot. It also depends on the frequency used for f_0 and on the stray capacitance in the experimental setup. For a glassy material of 1 μm film thickness, the theoretical error has a maximum of + 0.3% at fundamental frequency and the 3rd harmonic, and increases to about + 0.7% at the 5th harmonic. These results are based on calculations using eqs. (1b), (9) and (10) with the experimentally determined effective quartz parameters, including an external capacitance. Although these errors are very small and negligible for most applications, the shear modulus calculation is much more sensitive to deviations of the calculated film thickness from the real value. The more the acoustic load approaches the gravimetric regime, the greater the changes of the complex shear modulus, which are necessary to 'compensate' even very small errors in the calculated thickness to achieve the measured acoustic load (see Fig. 2). This mathematical coupling between film thickness and complex shear modulus is a major limitation in the film modulus determination with acoustic devices in the glassy state, and is more important than the experimental error in the impedance measurement. Note that all deviations are positive, i.e., the calculated film thickness is too thick.

In contrast to previously published investigations[9,21] we further adjusted the coating thickness with the full transmission line model at higher harmonics to account for the higher film thickness error. We assumed a glassy film consistency for the higher harmonics. As discussed in the Viscoelastic Material section, this assumption is reasonable because the material exhibits glassy behavior at the fundamental frequency at a measuring temperature of – 50°C.

5.2 *Shear parameter set of PIB*

The computation of the shear storage and the shear loss moduli of the polymer film was performed by fitting theoretically calculated curves directly to the reflection coefficient set, eq. (11), using eq. (8) for the electrical impedance, $\underline{Z}^e$. The fitting algorithm includes the following two steps.

A) In the first step, the effective quartz values, thickness, viscosity, and (electrode) area were determined using eq. (8) with $\zeta = 0$. This procedure requires an impedance analysis in the frequency range which includes both the serial and the parallel resonant frequency of the uncoated quartz. We used the complete data set of 801 measuring points for this part. The computation was performed at every temperature for the fundamental frequency as

well as for the third and fifth harmonics. An external capacitance, C_{ex}, parallel to C_0 was introduced into the equivalent circuit to account for parasitic capacitance. In contrast to C_0, this external capacitance does not influence the acoustic transmission line. From that data set, the quartz parameters $\underline{\alpha}_q$ and $\underline{K}_q^2$ can be calculated, leaving $\underline{Z}_p^*$ the only unknown variable.

B) In the second step, the unknown shear parameter set was determined from eq. (8) together with eqs. (4), (10) and (11). $\underline{G}$ cannot be extracted from the transcendental eq. (10) without approximations. Unfortunately there is no sufficiently accurate approximation of the tan function. The argument varies within the range shown in Fig. 2 from 0 to π (imaginary part) or 0 to $\pi/3$ (real part) at the fundamental frequency. A new method exploits different approximations of the tan function with different validity ranges, which all allow the separation and direct calculation of $\underline{G}$. An algorithm selects the best adapted approximation.[27]

In this study we use an optimized fitting procedure. At low quartz damping the procedure minimizes the average fitting error between the theoretically calculated reflection coefficient plots and the experimental values by changing G' and G''. The new version extracts 201 measuring points, centered about the zero phase serial resonant frequency of the coated resonator, equivalent to $\mathrm{Im}(\underline{S}_{11}) = 0$, in a preceding step. This method limits noise problems near the parallel resonance frequency, which occur particularly when the quartz is only slightly damped. If the quartz is highly damped and this serial frequency does not exist, the complete measuring curve is used. The program starts its search at a certain combination of G' and G'', compares the theoretical and the experimental values and tries new combinations of G' and G'' until the best fit is found. The direction and step width of the G'/G'' changes are automatically calculated from preceding steps. To illustrate the necessity of a sophisticated search algorithm, we calculated the complete fitting error field for some selected temperatures. Note, that the fitting algorithm calculates only the values along the search trace. Figure (4) shows as two examples, parts of the fitting field at 0°C and 120°C. The darker the gray, the smaller the complex error vector and the better the fit. Figure 4(b) shows a significant black dot at $G' = 2.8$ MPa and $G'' = 1.6$ MPa. The fitting algorithm has high accuracy. By contrast, the best-fit area in Fig. 4(a) has the shape of a needle. G' is well defined with 148 MPa but G'' generates an almost constant fitting error between $G'' = 10^1$ and 10^5 Pa. This unpropitious situation reflects the sensitivity of the acoustic load response to changes in G' and G'' as presented in Fig. 3 (white area in Fig. 3(b) for these moduli) and is the practical reason why we could not determine G'' values at low temperatures. The shear storage modulus values are still useful.

The $\underline{S}_{11}$ plots recalculated from the shear parameters coincide with the experimental results, except at high temperatures where the quartz is extremely damped. Here we found an increasing bias between the electrical admittance plot, $\underline{Y}^e$, calculated from the experimental results and the fitted data. We assume a calibration problem in the wire admittance. A small deviation of the calibration admittance parallel to the quartz influences the absolute values of $\underline{Y}^e$. Characteristic frequencies, such as the frequencies at $\mathrm{Im}(\underline{Y}^e) = \mathrm{Max}$,

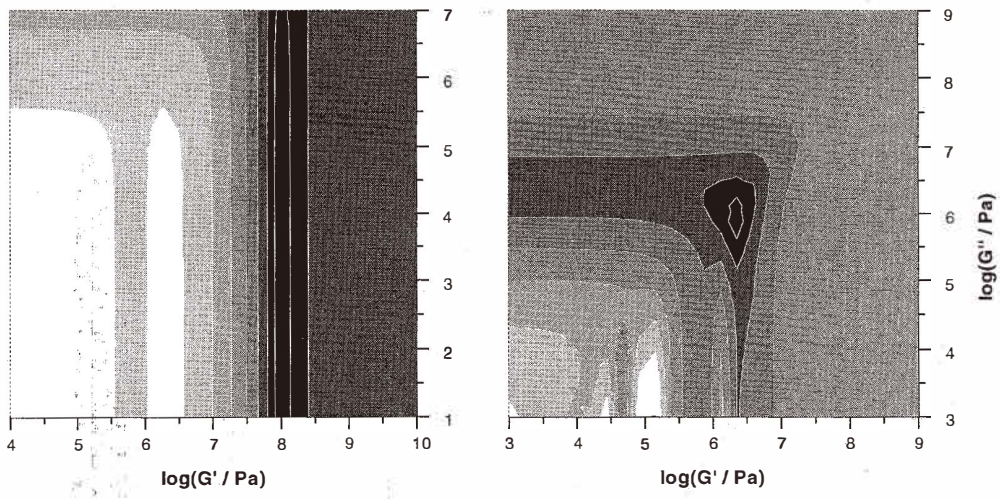

Fig. 4. Part of the fitting error field where the algorithm searches for the global error minimum between the experimental values from network analyzer measurements and theoretical values at two different temperatures corresponding to (a) the glassy state (0°C) and (b) the rubbery state (120°C). The darker the gray, the better the fit.

$\mathrm{Im}(\underline{Y}^e) = \mathrm{Min}$, or , $\dfrac{\mathrm{Im}(\underline{Y}^e)}{\mathrm{Re}(\underline{Y}^e)} = \mathrm{Max}$, remain unchanged. Under some approximations which can be applied under high acoustic load conditions, the motional load impedance, $\underline{Z}_{m,L}$, can be calculated from characteristic frequencies.

$$Z''_{m,L} = \frac{1}{2\omega C} - Z''_{m,q}(f) \qquad @\, f = f\left(\frac{\mathrm{Im}(\underline{Y}^e)}{\mathrm{Re}(\underline{Y}^e)} = \mathrm{Max}\right)$$

$$Z'_{m,L} = \left|Z''_{m,q}(f) + Z''_{m,L}\right| - Z'_{m,q}(f) \quad @\, f = f\left(\mathrm{Im}(\underline{Y}^e) = \begin{matrix}\mathrm{Max}\\ \mathrm{Min}\end{matrix}\right) \tag{12}$$

The complex shear modulus is subsequently determined with a fitting procedure to the acoustic load, $\underline{Z}_p^a$, which can be calculated from $\underline{Z}_{m,L}$ by the second term of eq. (9). The accuracy of this method depends mostly on the accuracy of the characteristic frequency determination.

We also included an empirical admittance into the equivalent circuit parallel to the quartz and determined the shear parameter set. The results are summarized in Fig. 5 and

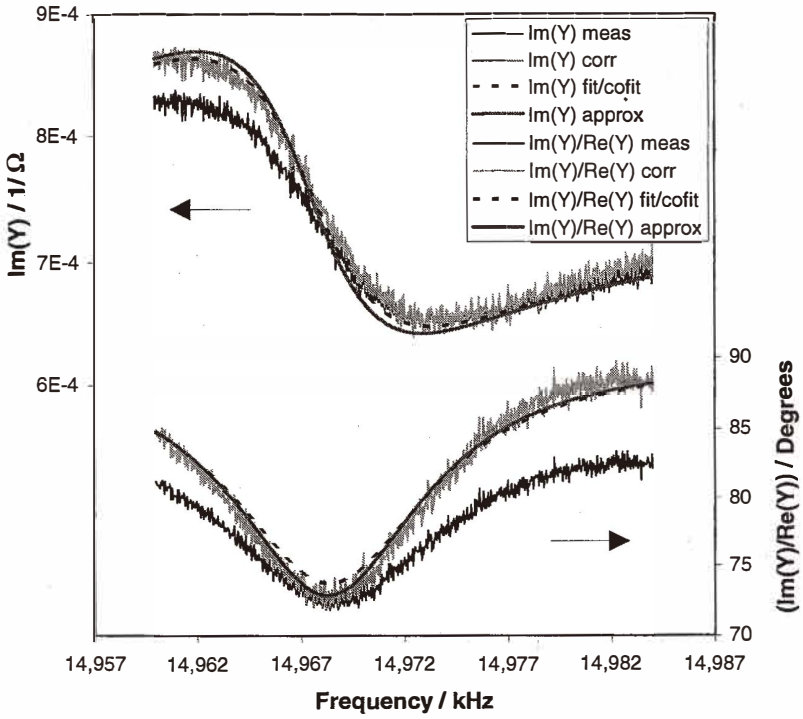

Fig. 5. $\mathrm{Im}(\underline{Y}^e)$ and $\mathrm{Im}(\underline{Y}^e)/\mathrm{Re}(\underline{Y}^e)$ calculated from $\underline{S}_{11}$ measurements with a network analyzer at 120°C without (meas) and with an empirical parallel admittance correction (corr), and the theoretical values recalculated from the respective complex shear moduli, $\underline{G}$ (fit, cofit, both curves overlap, and approx). The moduli were determined by a fitting procedure from the original $\underline{S}_{11}$ data set (fit) and from the data set corrected with the parallel admittance (corr), and the approximations, using eq. (12) (approx).

Table 1

Shear storage modulus, G', and shear loss modulus, G'', calculated by the fitting procedure from the original $\underline{S}_{11}$ measurements at 120°C (fit), from the $\underline{S}_{11}$ data set corrected with an empirical parallel admittance (corr) and from the approximations, using eq. (12) (approx).

	G'/MPa	G''/MPa
fit	8.366	9.072
corr	8.575	9.222
approx	8.845	9.427

Table 1 for the 120°C measurement at the third harmonic. The noisy curves are the plots calculated from the measured S_{11} parameter set without and with an additional parallel admittance. The smooth lines are the plots recalculated from the shear moduli in Table 1. They deviate only slightly from each other and fit quite well with the measurement plot which was corrected with the parallel admittance. The more important result is the acceptable difference of less than 6% between the G-values. Although the theoretical fit to the original data is significantly worse than that under low load conditions the shear modulus determination procedure is appreciably accurate. The G calculation from characteristic frequencies is also applicable.

Figure 6 presents the shear moduli and the loss tangent of PIB for the fundamental frequency at 5 MHz and the 3rd and 5th harmonics (15 MHz and 25 MHz, respectively). The results demonstrate the feasibility of shear parameter determination with quartz crystal resonators. The material undergoes a phase transition within the measurement range. The shear storage modulus decreases by two orders of magnitude. The shear loss modulus has

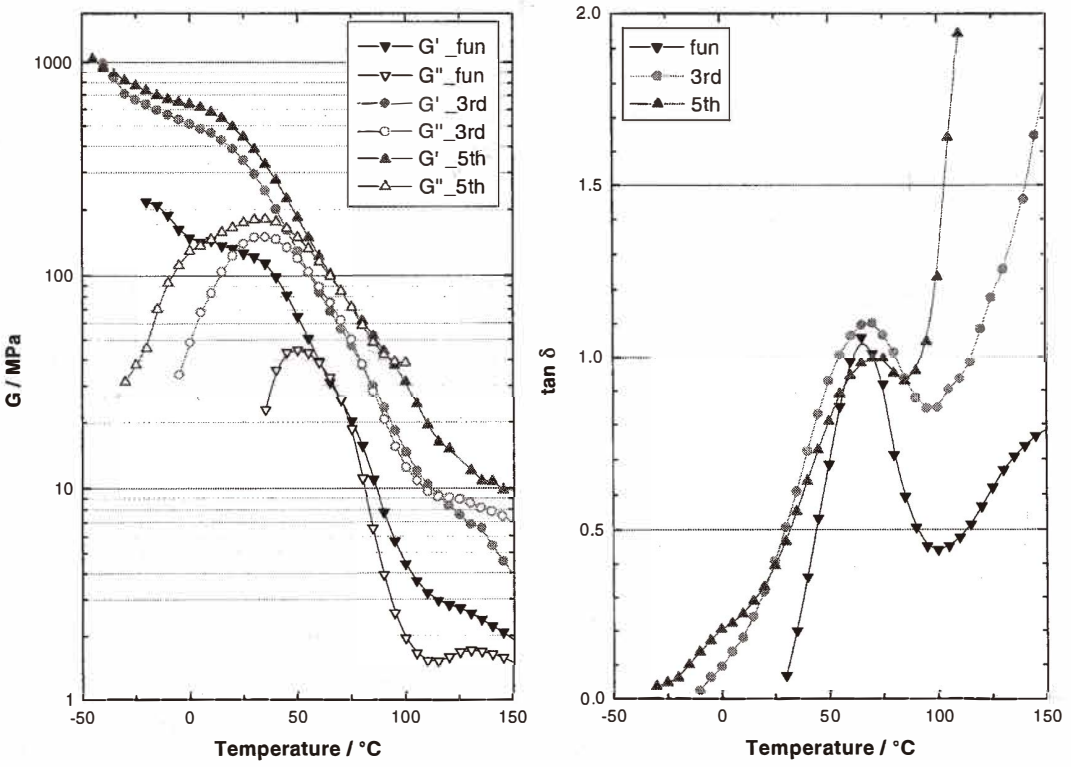

Fig. 6. Shear storage modulus, G', shear loss modulus, G'', and loss factor tan $\delta = G''/G'$ of PIB extracted with the full transmission-line model between –50 and 150°C.

a maximum, and the 'width' increases with the probing frequency. The loss factor has a maximum (fundamental frequency) or at least a shoulder (5th harmonic). The maxima in the loss factor correspond to a phase transition temperature of 65°C, 75°C or 80°C. The difference in the transition temperature to the static glass transition temperature is more than 130°C. The transition area is very broad (about 100°C) when running through a temperature regime.

As mentioned already, the coating thickness cannot be optimized for glassy and rubbery films at the same time for all measuring frequencies. In the lower temperature range, our film approaches the gravimetric regime, i.e., the film is too thin, and the acoustic impedance is almost $\underline{G}$ independent. In the temperature range above 100°C the quartz oscillation at higher harmonics is highly damped. The theoretically calculated curves do not perfectly coincide with the experimental curves as found for the other data points. The film is now too thick to obtain optimal results. This is why we do not want to overinterpret the results obtained at the fundamental frequency under the glassy film consistency and at higher harmonics for a rubbery film.

However, the shoulders in the G' curves below 0°C and the increase of tan δ at high temperatures are significant and can be found even with a slightly varied film thickness, indicating a material effect. It will be analyzed in a separate investigation.

Figure 7 shows the transition temperatures determined from our acoustic measurements with other mechanically determined values available from the literature.[17,28] The data from calorimetric investigations ($\kappa C_p''$) are added for comparison. Our data are significantly lower (in terms of frequency) or higher (in terms of transition temperature) than McCrum *et al.*'s determined from G'' measurements.[17] The same applies for Donth *et al.*'s values calculated from tan δ measurements at low frequencies.[28] As is well known, the tan δ peaks are shifted to lower frequencies when compared to the G'' peaks. Donth *et al.* also distinguish between two different transition phenomena, the α relaxation (open squares) and the $c\beta$ relaxation (full squares). The PIB master plot shows a main maximum and a second shoulder on the high-frequency side. The α- and cβ-relaxation phenomena are assumed to be related to large-scale and small-scale glass transitions, respectively. The local process is also called a "cooperative β relaxation."[28] Unfortunately, the frequency difference between the acoustic and the mechanical experiments is very large. At the moment we cannot decide whether our results have a common trace with one of the low frequency experiments.

We also have no indication of systematic errors in our experiment except the limitations discussed already. A systematic error could arise from cross-film inhomogeneities as reported by Bandey *et al.*[29] In contrast to our experiments they used a quartz crystal with a rough surface. Here, the part of a polymer layer attached to the surface behaves like a rigidly coupled material due to surface roughness. Only the outer layer exhibits viscoelasticity. We should, however, mention that at least the part of the thin film in direct contact with a solid surface does not necessarily behave like a bulk material or a free thin film. Owing to interfacial forces at the quartz substrate/film interface, the molecular mobility can be decreased. Strong adhesion would be expected to have an effect similar to that of cross-linking on bulk specimens. The chain connectivity extends the influence of the surface much farther into the film than a few segment lengths. Wallace *et al.* reported on

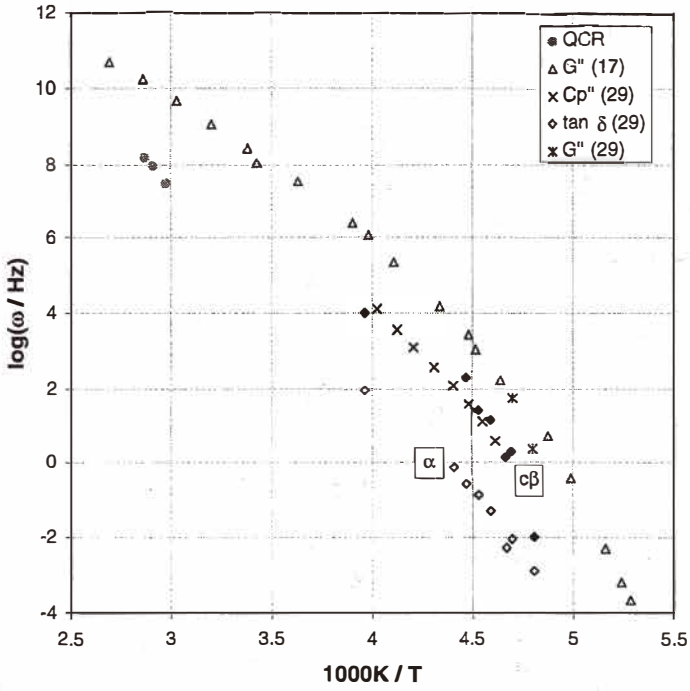

Fig. 7. Arrhénius plot of the main transition of PIB determined from different measurements: mechanical tan δ, separated into α-relaxation (open squares) and cβ (full squares),[29] shear loss mofulus (triangles)[17] (stars),[29] calorimetric (crosses),[29] and acoustic (full circles).

thermal expansion coefficient observations of polystyrene.[30] They found a T_g shift of at least 60 K for thin films up to 400 Å and 25 K for a 200 nm film.

It is beyond the scope of this work to elaborate on those discussions; however, the capability of the acoustic method to provide additional information on the mechanical properties of thin films in the high-frequency range is clear.

6. Conclusions

The analysis of the electrical impedance of a coated quartz crystal resonator with a network analyzer is a feasible method of determining the shear storage and shear loss modulus of thin polymer films at high probing frequencies. Changes in material properties result in changes in the electrical impedance of the coated quartz crystal via changes in the acoustic impedance of the film. The physical background of acoustic wave propagation in

a multilayer structure can be modeled successfully in a one-dimensional transmission line model. The experimental design must be optimized regarding the relationship between probing frequency and coating thickness, as well as the shear storage and shear loss modulus and complex acoustic load.

Acknowledgments

This work was supported by the Ministry of Education and Research (BMBF) under contract 16 SV070/3 and the German Research Foundation under Contract Lu605/2-1. The authors are grateful to Stephen J. Martin and Richard W. Cernosek from Sandia National Laboratories, Albuquerque, for providing assistance in performing the experiments, and Klaus Schröter from the Martin Luther University for the mechanical data and helpful discussions.

References

1 G. Sauerbrey: Z. Physik **155** (1955) 206.
2 S. Bruckenstein and M. Shay: Electrochim. Acta **30** (1985) 1295.
3 K. K. Kanazawa and J. G. Gordon: Anal. Chem. **57** (1985) 1770.
4 S. J. Martin, V. E. Granstaff and G. C. Frye: Anal. Chem. **63** (1991) 2272.
5 S. J. Martin, G. C. Frye and K. O. Wessendorf: Sensors and Actuators A **44** (1994) 209.
6 S. J. Martin and G. C. Frye: IEEE Ultrasonics Symp. (1991) 393.
7 A. Katz and M. D. Ward: J. Appl. Phys. **80** (1996) 4153.
8 A. Dormack and D. Johannsmann: J. Appl. Phys. **80** (1996) 2599.
9 R. Lucklum, C. Behling, R. W. Cernosek and S. J. Martin: J. Phys. D: Appl. Phys. **30** (1997) 346.
10 J. W. Grate, S. N. Kaganove and V. R. Bhethanabotla: Faraday Discuss. **107** (1997) 259.
11 R. Lucklum, C. Behling and P. Hauptmann: 1997 Joint International Meeting, Electrochemical Society Proceedings, Volume 97–19 (Pennington, NJ, 1997) p. 236.
12 R. Lucklum, C. Behling and P. Hauptmann: 7th Int. Meeting on Chem. Sensors 1998, Techn. Digest (Int. Academic Press, Beijing 1998) p. 121.
13 R. Lucklum, C. Behling and P. Hauptmann: Anal. Chem. (1999) in print.
14 J. D. Ferry: Viscoelastic Properties of Polymers (John Wiley & Sons, New York, 1980) Chaps. 1,2,11,12,13,15.
15 J. J. Aklonis and W.J. MacKnight: Introduction to Polymer Viscosity (John Wiley & Sons, New York, 1983) Chaps. 2,3,4.
16 M. L. Williams, R. F. Landel and J. D. Ferry: J. Amer. Chem. Soc. **77** (1955) 3701.
17 N. G. McCrum, B. E. Reed and G. Williams: Anelastic and Dielectric Effects in Polymeric Solids (John Wiley & Sons, New York, 1967) Chap. 10.4.
18 E. Benes, M. Schmidt and V. Kravchenko: J. Acoust. Soc. Am. **90** (1991) 700.
19 R. Lucklum, S. Schranz, C. Behling, F. Eichelbaum and P. Hauptmann: Sensors and Actuators A **60** (1997) 40.
20 S. Schranz and P. Hauptmann: Tagungsband 3. Chemnitzer Fachtagung Mikrosystemtechnik (Chemnitz, 1997) S. 9.
21 R. Lucklum and P. Hauptmann: Faraday Discuss. **107** (1997) 123.
22 O. Wolff, E. Seydel and D. Johannsmann: Faraday Discuss. **107** (1997) 91.
23 R. Krimholtz, D. A. Leedom and G. L. Mathaei: Electron. Lett. **6** (1970) 398.

24 C. Behling, R. Lucklum and P. Hauptmann: Sensors and Their Applications VII (IOP, Bristol, 1995) p. 370.
25 R. Lucklum, C. Behling and P. Hauptmann: Sensors and Actuators A **66/1–3** (1998) 184.
26 V. E. Granstaff and S. J. Martin: J. Appl. Phys. **75** (1994) 1319.
27 C. Behling, R. Lucklum and P. Hauptmann: 1998 IEEE International Frequency Control Symposium, Pasadena (CA), Proceedings (Inst. Electrical & Electronics Engineers, Inc., Piscataway, NJ, 1998) p. 823.
28 E. Donth, M. Beiner, S. Reissig, J. Korus, F. Garwe, V. Vieweg, S. Kahle, E. Hempel and K. Schröter: Macromol. **29** (1996) 6589.
29 H.L. Bandey, A. R. Hillman, M. J. Brown and S. J. Martin: Faraday Discuss. **107** (1997) 105.
30 W. E. Wallace, J. H. van Zanten and W. L. Wu: Phys. Rev. E **52** (1995) R3329.